Dynamic Energy Flow Analysis of Integrated Gas and Electricity Systems using the Holomorphic Embedding Method

Tong Zhang[a,b], Zhigang Li[a,*], Qiuwei Wu[c], Shixian Pan[a], Q. H. Wu[a]

[a]*School of Electric Power Engineering, South China University of Technology, Guangzhou 510640, China*
[b]*School of Engineering, Cardiff University, Cardiff CF24 3AA, UK*
[c]*Center for Electric Power and Energy, Technical University of Denmark, Kgs. Lyngby 2800, Denmark*

Abstract

To perform efficient simulation of the integrated gas and energy system's operation and explore the interaction between natural gas and electric power, an energy flow analysis tool with high accuracy and computational efficiency is needed. The commonly used steady-state analysis method is not applicable in computing the pipeline dynamics of natural gas networks, and it is computationally expensive for most transient analysis methods to obtain high-resolution solutions. In addition, conventional methods generate energy flow profiles at pre-set time intervals, which are not compatible with continuous-time applications. To bridge these gaps, this paper proposes a dynamic energy flow analysis method applied in integrated gas and electricity systems using the holomorphic embedding method. The system's state equations are formulated using ordinary differential equations based on a simplified natural gas network model and are reconstructed by time-embedded holomorphic functions. By solving these functions, the continuous-time profiles of the energy flow of the whole system can be readily generated with a moderate computational burden, and the pipeline dynamics can be addressed. The simulation results of the case studies validate the improved computational performance of the proposed method over that of a conventional ordinary difference equation solver. In both small-scale and large-scale cases, the proposed method can capture the transient process in every state variable in response to disturbances accurately and efficiently.

Keywords: Energy flow analysis, Holomorphic embedding method, Integrated gas and electricity system, Pipeline dynamics

1. Introduction

With the increasing demand for flexibility caused by the growing proportion of intermittent renewable energy, natural gas (NG) in the power supply sector has been increasingly important for decades. In the UK, natural gas has been pivotal to electricity generation,

*Corresponding author
Email address: lizg16@scut.edu.cn (Zhigang Li)

providing approximately 30 percent of fuel in 2020 [1]. In the United States, natural gas has represented more than 25 percent of all primary energy consumption during the past decade [2]. This trend has propelled the integration of NG facilities into power systems, from gas-fired generators to power-to-gas equipment, resulting in the development of integrated gas and electricity systems (IGESs) in terms of both scale and complexity. To keep the operation of an IGES secure and economical, it is necessary to perform a comprehensive, accurate and efficient energy flow analysis (EFA) for the entire system.

The EFA lays a foundation for other applications, including planning [3, 4], optimal operation [5, 6], and reliability assessment [7, 8]. The objective of an EFA is to obtain the operating states of an IGES based on the known network configurations and demand/supply data. It provides the system operators with comprehensive knowledge of the gas flow rates, nodal pressures and nodal voltages of the IGES, and reflects the evolution of the system's states in response to changes in operating conditions. Many studies on IGESs employ steady-state natural gas network (NGN) models to reduce the modelling complexity [9, 10, 11]. However, the steady-state models do not consider the pipeline dynamics and cannot depict the IGES's evolution when a disturbance occurs. Especially when the system is faced with abrupt changes, operating states are likely to oscillate in a short time period. Failure to capture this intermediate transient process might cause obvious computation deviations, which may lead to inappropriate actions taken by the system operators. Therefore, a continuous-time EFA method that precisely describes pipeline dynamics should be adopted in the EFA.

In recent years, more advanced models have been adopted instead, i.e., steady-state models considering linepack [12], quasi-dynamic models [13] and transient models [14, 15]. In pursuit of higher fidelity, transient models are drawing increasing attention. For the transient analysis of NG sectors in IGESs, the gas propagation along each pipeline is depicted using a one-dimensional isothermal model, which is represented by partial differential equations (PDEs) [16], and various methods have been utilized to solve PDEs. Numerical methods are commonly used, including the method of characteristics [17], the finite element method [18], the finite difference method (FDM) [19, 20] and the finite volume method [16]. There are some advanced methods that have been recently proposed, including the improved FDM [21] and also some intelligent algorithms [22] using training data obtained by FDM. However, the accuracy of these methods depends on the resolution of spatial and temporal discretization, and sometimes the pursuit of higher fidelity may cause a heavy computational burden. As an alternative, the Laplace transform method [23] has difficulties handling nonlinear items in NGN equations. Converting PDEs into ordinary differential equations (ODEs) is used as well [24, 25]. In the electric analogy method, a set of first-order ODEs are generated based on the analogous model of resistance and capacitance in electric circuit theory [26]. There are also other ODE-based models of NGN [27][28] that have accuracy comparable to the PDE model, but are mainly used in the optimization problems (i.e., the optimal control of gas compressors and the economic dispatch of IGESs). A linepack depletion model for NGNs is developed based on three alternative ODE simulations, effectively characterizing the survival time of NGNs under contingencies [29]. The outputs of most current dynamic simulation methods are still discrete-time profiles of system operation at pre-set time inter-

vals rather than continuous-time depictions. When fine-resolution profiles of energy flow are required, these methods need to either estimate the energy flow using interpolation or perform computation frequently. When a transient model of NGNs is adopted, the increasing computational complexity makes it challenging to balance accuracy and efficiency.

Recently, the holomorphic embedding method (HEM) has been developed to perform fast computation with better convergence and competent accuracy [30, 31]. In addition to power flow analysis [32, 33], voltage stability assessment [34] and network equivalents [35], the HEM has been explored in applications including the dynamic simulation of power systems. In [36], a holomorphic embedding formulation of an induction motor model in the time domain is developed and applied in power systems to perform voltage stability analysis. In [37], the HEM-based approach is extended to the dynamic simulation of power systems under faults involving a set of differential algebraic equations (DAEs). The application of HEM has been extended into the optimization of integrated distribution energy systems [38] and the steady-state analysis of IGES [39]. However, the possibility of employing this method in the dynamic EFA of the NG sectors has not been explored yet. HEMs have great potential in solving ODE or DAE problems of power systems and have been proved applicable in steady-state NGN computation, which may shed some light on the transient analysis of pipeline networks such as NGNs.

In this paper, a novel EFA method for IGESs with transient NGN models is developed based on the idea of the HEM, which will help obtain detailed dynamic process of IGES. First, the IGES model consisting of the steady-state electric power system (EPS) model, the transient NGN model and coupling units is formulated by incorporating the ODEs into the NGN model. Then, the IGES energy flow equations are reformulated by embedding a set of time-dependent holomorphic functions. A recursive procedure for solving the unknown coefficients of holomorphic functions and a multistage computation scheme for dynamic simulation are developed. The proposed method is tested in two IGES cases with different operating conditions and analysed in terms of accuracy and speed. The contributions of this paper are summarized as follows:

1. An IGES model is reformulated using holomorphic functions based on the idea of holomorphic embedding. Compared with our previous work [39], this paper adopts an ODE-based transient NGN model considering the dynamics of NG pipelines, and time-dependent holomorphic functions are used to reflect the time-varying operating states of an IGES.

2. A dynamic gas flow analysis method is developed, incorporating a recursive solving procedure and a multistage computation scheme. To the best of our knowledge, this is the first attempt to extend the HEM to the solution of dynamic energy flow analysis of NGNs. Compared with other recently-proposed methods, this method avoids the temporal discretization and only needs to solve algebraic equations during the whole calculation, producing accurate results while maintaining a low computational complexity.

3. A combined dynamic energy flow analysis algorithm for IGESs is proposed and tested

under different operating conditions. This method yields an accurate continuous-time profiling of IGES energy flow, reflecting the transient process after a disturbance occurs.

The remainder of this paper is organized as follows: Section II formulates the IGES model for transient NGN models. Section III develops the HEM formulations and solution procedures for IGESs. Case studies are performed in Section IV to evaluate the computational capability of the proposed method. Finally, conclusions are given in Section V.

2. Modelling of Integrated Gas and Electricity Systems

An IGES consists of EPSs, NGNs, and the coupling units connecting these two sectors (as shown in Fig. 1). In an NGN, natural gas is supplied by gas wells or storage facilities, transported via pipelines and delivered to consumers. In an EPS, power is generated by generation units and delivered to consumers through transmission lines. The power and gas sectors are interconnected by coupling units such as gas-fired generators, power-consuming compressors, and power-to-gas equipment.

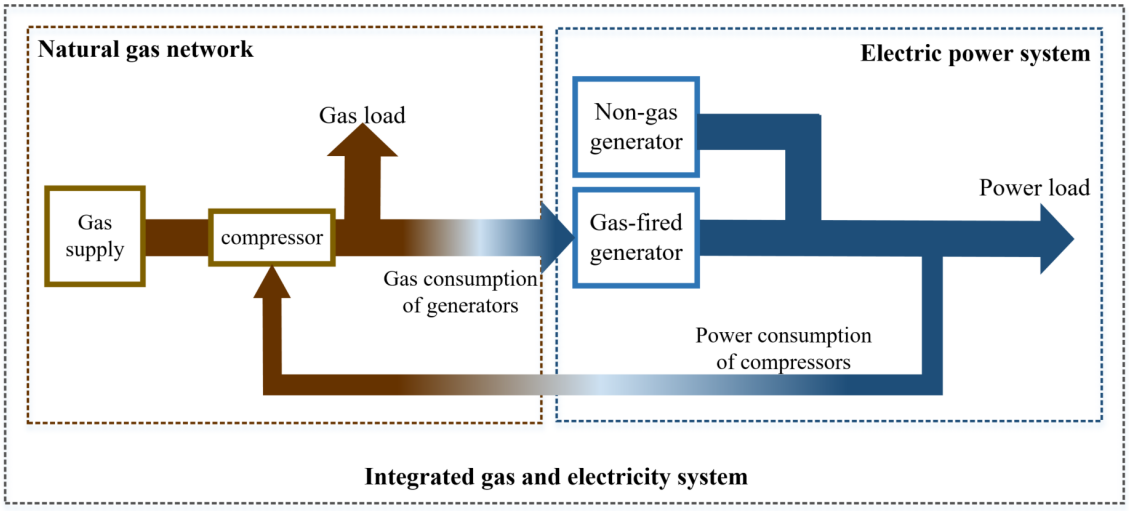

Figure 1: The configuration of an IGES

2.1. Dynamic Modelling of Natural Gas Networks

In this section, descriptions of single-pipe gas flow equations and multi-pipe network constraints are presented to build a comprehensive NGN model.

2.1.1. Single-Pipe Equations

The gas flow inside a pipe can be described by isothermal Euler equations. Assuming that the environmental temperature is fixed and the pipeline is horizontal, the mass conservation

and momentum balance equations can be written as:

$$\frac{\partial p}{\partial t} = -\frac{c^2}{A}\frac{\partial M}{\partial x}, \tag{1}$$

$$\frac{\partial M}{\partial t} = -A\frac{\partial p}{\partial x} - \frac{\lambda c^2}{2AD}\frac{M^2}{p}, \tag{2}$$

where p and M represent the gas pressure and gas flow rate along this pipe, respectively, and both variables are functions of time t and length x; D, A, λ and c represent the pipe diameter, pipe cross-sectional area, pipe roughness and sound velocity in gas, respectively.

The boundary conditions are set on the basis of $p(t,0) = p_0(t)$, $M(t,0) = M_0(t)$, $p(t,L) = p_L(t)$ or $M(t,L) = M_L(t)$ (the subscripts 0 and L represent the inlet and outlet of the pipe) based on the actual operation setting [27].

Using spatial discretization, we divide a pipeline of length L into N segments with the length of each segment being $l_n = L/N$ (as shown in Fig. 2). The gas flow rates at the inlet and outlet of each segment (for example, segment b) are denoted as M_b^{in} and M_b^{out}, respectively. The pressures on the inlet and outlet of each segment are denoted as p_b^{in} and p_b^{out}.

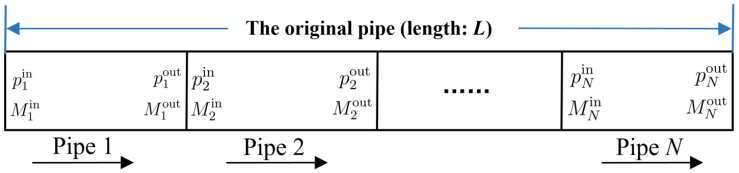

Figure 2: The configuration of the gas pipeline's spatial discretization

By integrating the partial differential terms p and M with respect to the distance l using the trapezoid rule, (1) and (2) can be converted into an ODE form, with derivatives of time t only [29]. The equations for an individual segment of the pipeline can be written as follows:

$$\frac{1}{2}\left(\frac{\mathrm{d}p_b^{\text{in}}}{\mathrm{d}t} + \frac{\mathrm{d}p_b^{\text{out}}}{\mathrm{d}t}\right) = \frac{c^2}{A_b l_b}\left(M_b^{\text{in}} - M_b^{\text{out}}\right), \tag{3}$$

$$\frac{1}{2}\left(\frac{\mathrm{d}M_b^{\text{in}}}{\mathrm{d}t} + \frac{\mathrm{d}M_b^{\text{out}}}{\mathrm{d}t}\right) = \frac{A_b}{l_b}\left(p_b^{\text{in}} - p_b^{\text{out}}\right) - \frac{\lambda c^2}{4A_b D_b}\frac{\left(M_b^{\text{in}} + M_b^{\text{out}}\right)^2}{p_b^{\text{in}} + p_b^{\text{out}}}. \tag{4}$$

2.1.2. Multi-pipe Network Modelling

A multi-pipe NGN model is constructed from pipelines, nodes and compressors. Natural gas is supplied at source nodes (by gas wells or gas storage stations) and transported via pipelines to local gas consumers. Considering the long distances between nodes in some large-scale NGNs, compressors are commonly installed to compensate for the pressure loss due to the friction inside the pipelines.

For each node, the gas flow balance of inflowing and outflowing pipelines should be maintained. With the gas demand at each node written as $M_{i,t}^{\mathrm{D}}$ and the gas supply at each node written as $M_{i,t}^{\mathrm{S}}$, the flow balance equation can be written as:

$$\sum A_{i,b}^{\mathrm{in}} M_{b,t}^{\mathrm{in}} + \sum A_{i,b}^{\mathrm{out}} M_{b,t}^{\mathrm{out}} = M_{i,t}^{\mathrm{S}} - M_{i,t}^{\mathrm{D}}, \quad \forall i \in \mathcal{I}^{\mathrm{NGN}}, \forall b \in \mathcal{P}^{\mathrm{NGN}}, \forall t \in \mathcal{T}, \tag{5}$$

where $M_{i,t}^{\mathrm{S}}$ and $M_{i,t}^{\mathrm{D}}$ are the supply and demand on Node i at time t; $A_{i,b}^{\mathrm{in}}$ and $A_{i,b}^{\mathrm{out}}$ are the nodal-line incidence matrix elements for inflowing and outflowing pipelines, respectively; $\mathcal{I}^{\mathrm{NGN}}$ and $\mathcal{P}^{\mathrm{NGN}}$ are the index collections of nodes and pipelines in NGNs, respectively; and $\mathcal{T}$ is the index collection of time periods.

For modelling pipelines installed with compressors, two nodes are added at the inlet and outlet of the compressor, dividing the original pipeline into three segments. As shown in Fig. 3, Pipe b_3 is a virtual pipeline with no actual length, while the other two segments, Pipe b_1 and Pipe b_2, replace the original pipeline and maintain the same gas dynamic characteristics. The pressure at the outlet of a compressor is proportional to the pressure at the inlet of the compressor, described as:

$$p_{k_1,t} = R_{b,t}^{\mathrm{C}} p_{k_2,t}, \quad \forall t \in \mathcal{T}, \forall b \in \mathcal{P}^{\text{NGN-COMP}}, \tag{6}$$

where k_1 and k_2 are the node indices of the inlet and outlet of the compressor on Pipe b, respectively; $p_{k_1,t}$ and $p_{k_2,t}$ are the inlet pressure and outlet pressure of the compressor, respectively; $R_{b,t}^{\mathrm{C}}$ is the compression ratio; and $\mathcal{P}^{\text{NGN-COMP}}$ is the index collection of pipelines equipped with compressor in NGNs.

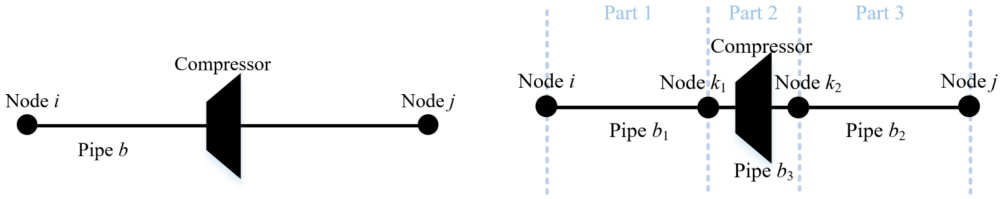

(a) Original pipeline (b) Newly-discretized pipeline

Figure 3: The modelling of a compressor-equipped pipeline in the natural gas network

For networks with more than one source, there is at least one node with multiple inflowing pipelines (denoted as the "infuse" node). In such a case, an additional constraint is needed to enable gas flow analysis. The outlet pressure for each pipe that flows into the same "infuse" node should remain the same. With $\frac{\mathrm{d}p_b^{\mathrm{out}}}{\mathrm{d}t} = \frac{2c^2}{A_b l_b}\left(M_b^{\mathrm{in}} - M_b^{\mathrm{out}}\right) - \frac{\mathrm{d}p_b^{\mathrm{in}}}{\mathrm{d}t}$ from (3), the constraint for an "infuse" node with two inflowing pipes (b_1 and b_2) can be written as:

$$\frac{2c^2}{A_{b_1} l_{b_1}}\left(M_{b_1}^{\mathrm{in}} - M_{b_1}^{\mathrm{out}}\right) - \frac{\mathrm{d}p_{b_1}^{\mathrm{in}}}{\mathrm{d}t} = \frac{2c^2}{A_{b_2} l_{b_2}}\left(M_{b_2}^{\mathrm{in}} - M_{b_2}^{\mathrm{out}}\right) - \frac{\mathrm{d}p_{b_2}^{\mathrm{in}}}{\mathrm{d}t}. \tag{7}$$

Combined with boundary conditions for the ODE-form equations ((3), (4) and (7)) and the algebraic equations ((5) and (6)) for the NGN constraints, the multi-pipe model can be depicted as a set of DAEs.

2.2. Steady-State Modelling of Electric Power Systems

The time scale of an EPS is small due to the fast transmission of electromagnetic and mechanical-electrical disturbances, making the transient process of electric power systems much shorter than that of NGNs [40]. Hence, a steady-state power flow model is capable of depicting the operation state of an EPS in the combined analysis of IGESs. The steady-state model of an EPS is represented by the following equations:

$$V_i \sum_{j \in \mathcal{I}^{\mathrm{EPS}}} V_j (G_{ij} \cos\theta_{ij} + B_{ij} \sin\theta_{ij}) = P_i^{\mathrm{G}} - P_i^{\mathrm{L}}, \quad \forall i \in \mathcal{I}^{\mathrm{EPS}}, \tag{8}$$

$$V_i \sum_{j \in \mathcal{I}^{\mathrm{EPS}}} V_j (G_{ij} \sin\theta_{ij} - B_{ij} \cos\theta_{ij}) = Q_i^{\mathrm{G}} - Q_i^{\mathrm{L}}, \quad \forall i \in \mathcal{I}^{\mathrm{EPS}}, \tag{9}$$

where P_i^{G} and P_i^{L} represent the active power generation and consumption, respectively; Q_i^{G} and Q_i^{L} represent the reactive power generation and consumption at Bus i, respectively; G_{ij} and B_{ij} are the elements in the conductance matrix and susceptance matrix, respectively; and $\mathcal{I}^{\mathrm{EPS}}$ is the index collection of buses in the EPS.

2.3. Coupling Units

The connection between the NG sector and the EP sector is usually made by electricity-consuming compressors, gas-fired turbines and power-to-methane equipment.

Assumed that the power consumed by the compressor on Pipe b is supplied by Bus i, then the power consumption can be calculated using the equation :

$$P_{i,t}^{\mathrm{C}} = C_{b,t}^{\mathrm{C}} M_{b,t}^{\mathrm{C}}, \quad \forall t \in \mathcal{T}, \tag{10}$$

where $C_{b,t}^{\mathrm{C}}$ is a constant representing the composition of the supercompressibility factor, compressor parasitic efficiency, nodal temperature, specific heat ratio of natural gas, compression process efficiency, etc.; $M_{k,t}^{\mathrm{C}}$ is the gas flow rate through the pipe equipped with compressor k.

For a gas-fired turbine at Node k that supplies the generator at Bus i in the EPS, its gas consumption can be calculated using the equation below:

$$M_{k,t}^{\mathrm{GT}} = \alpha_i \left(P_{i,t}^{\mathrm{GT}}\right)^2 + \beta_i P_{i,t}^{\mathrm{GT}} + \gamma_i, \quad \forall t \in \mathcal{T}, \tag{11}$$

where $M_{k,t}^{\mathrm{GT}}$ and $P_{k,t}^{\mathrm{GT}}$ are the turbine's gas consumption and power output; α, β and γ are the coefficients of the gas consumption.

For a power-to-methane equipment supplied by Bus i, the methane output is proportional to the power consumption, which can be calculated using the equation below:

$$M_{i,t}^{\mathrm{P2M}} = C_{i,t}^{\mathrm{P2M}} P_{i,t}^{\mathrm{P2M}}, \quad \forall t \in \mathcal{T}, \tag{12}$$

where $M_{i,t}^{\mathrm{P2M}}$ and $P_{i,t}^{\mathrm{P2M}}$ are methane output and power consumption; $C_{i,t}^{\mathrm{P2M}}$ is the transfer ratio.

Incorporating the DAEs representing the natural gas sector, Equations (8) and (9) for the electric power sector, and Equations (10) to (12) for the coupling units, the IGES model that covers the transient analysis of the NGN and the steady-state analysis of the EPS can be described by a DAE system.

3. Holomorphic Embedding Solution for Integrated Gas and Electricity Systems

The idea of an HEM is to embed the original problem into a larger problem and to calculate the unknown variables by solving the larger problem. The HEM-based method includes the following three steps for solving energy flow equations:

1. Constructing the larger problem: reformulating the energy flow equations by replacing the unknown variables with holomorphic functions of the time variable t.

2. Solving the larger problem: calculating the unknown coefficients in the holomorphic functions in the larger problem and obtaining a known holomorphic polynomial function of t.

3. Evaluating the states: putting t into the known holomorphic functions to evaluate the unknown variables.

The details of the aforementioned three steps are given in the next sub-sections.

3.1. HE Formulation and Solution of the NGN

3.1.1. HE Reformulation of the NGN Equations

To construct the larger problem, the original NGN equations are reformulated by substituting the time-dependent variables M and p with holomorphic functions of time t represented by $M_b^{\text{in}}(t)$, $M_b^{\text{out}}(t)$, $p_b^{\text{in}}(t)$ and $p_b^{\text{out}}(t)$. The holomorphic functions can be replaced by their Tayplor series when t is within a certain neighbouthood [41], hence are written in the following forms:

$$M_b^{\text{in}}(t) = \sum_{n=0}^{\infty} M_b^{\text{in}}[n] t^n, \tag{13}$$

$$M_b^{\text{out}}(t) = \sum_{n=0}^{\infty} M_b^{\text{out}}[n] t^n, \tag{14}$$

$$p_b^{\text{in}}(t) = \sum_{n=0}^{\infty} p_b^{\text{in}}[n] t^n, \tag{15}$$

$$p_b^{\text{out}}(t) = \sum_{n=0}^{\infty} p_b^{\text{out}}[n] t^n, \tag{16}$$

where $M_b^{\text{in}}[n]$, $M_b^{\text{out}}[n]$, $p_b^{\text{in}}[n]$, and $p_b^{\text{out}}[n]$ are the coefficients of the t^n terms in the holomorphic functions. The HEM-form gas flow equations are reformulated by embedding them into the original NGN equations (Equations (3) to (7)).

Equation (4) is further rewritten in the form below:

$$\frac{\mathrm{d}M_b^{\text{in}}(t)}{\mathrm{d}t} + \frac{\mathrm{d}M_b^{\text{out}}(t)}{\mathrm{d}t} = \frac{2A_b}{l_b}\left(p_b^{\text{in}}(t) - p_b^{\text{out}}(t)\right) - \frac{\lambda c^2}{2A_b D_b}\left(M_b^{\text{in}}(t)\right)^2 r_b(t), \quad \forall b \in \mathcal{P}^{\text{NGN}}, \tag{17}$$

where $r_b(t)$ is the inverse of $\left(p_b^{\text{in}}(t) + p_b^{\text{out}}(t)\right)$: $r_b(t) = \frac{1}{p_b^{\text{in}}(t)+p_b^{\text{out}}(t)}$ (the nodal pressures are non-zero variables). $r_b(t)$ is represented by the Taylor series expansion of t as well: $r_b(t) = \sum_{n=0}^{\infty} r_b\,[n]\,t^n$.

The derivatives of $M_b^{\text{in}}(t)$, $M_b^{\text{out}}(t)$, $p_b^{\text{in}}(t)$ and $p_b^{\text{out}}(t)$ with respect to t are expressed by:

$$\frac{\mathrm{d}M_b^{\text{in}}}{\mathrm{d}t} = \sum_{n=1}^{\infty} \left(n \cdot M_b^{\text{in}}\,[n]\,t^{n-1}\right), \tag{18}$$

$$\frac{\mathrm{d}M_b^{\text{out}}}{\mathrm{d}t} = \sum_{n=1}^{\infty} \left(n \cdot M_b^{\text{out}}\,[n]\,t^{n-1}\right), \tag{19}$$

$$\frac{\mathrm{d}p_b^{\text{in}}}{\mathrm{d}t} = \sum_{n=1}^{\infty} \left(n \cdot p_b^{\text{in}}\,[n]\,t^{n-1}\right), \tag{20}$$

$$\frac{\mathrm{d}p_b^{\text{out}}}{\mathrm{d}t} = \sum_{n=1}^{\infty} \left(n \cdot p_b^{\text{out}}\,[n]\,t^{n-1}\right). \tag{21}$$

For the germ solution of the reformulated NGN equations, $M_b^{\text{in}}[0]$, $M_b^{\text{out}}[0]$, $p_b^{\text{in}}[0]$ and $p_b^{\text{out}}[0]$ are set according to the boundary conditions. $r_b[0]$ is calculated by the following equation:

$$r_b[0] = -\frac{1}{p_b^{\text{in}}[0] + p_b^{\text{out}}[0]}. \tag{22}$$

3.1.2. Recursive Procedure for Solving Holomorphic Functions in NGNs

The reformulated NGN equations are built from the holomorphic polynomials of t and therefore contain coefficients corresponding to the t^n terms of different orders. To calculate the unknown coefficients in the holomorphic functions, a recursive procedure is adopted in this section.

Compare the coefficients for all t^k terms, and a set of equations containing $M_b^{\text{in}}[n]$, $M_b^{\text{out}}[n]$, $p_b^{\text{in}}[n]$, $p_b^{\text{out}}[n]$ and $r_b[n]$ $(n \leq k)$ are obtained:

$$p_b^{\text{in}}[k] + p_b^{\text{out}}[k] = \frac{2c^2}{kA_b l_b}\left(M_b^{\text{in}}([k-1] - M_b^{\text{out}}[k-1]\right), \quad \forall b \in \mathcal{P}^{\text{NGN}}, \tag{23}$$

$$\begin{aligned} &M_b^{\text{in}}[k] + M_b^{\text{out}}[k] = \frac{2A_b}{kl_b}\left(p_b^{\text{in}}[k] - p_b^{\text{out}}[k]\right) \\ &-\frac{\lambda c^2}{2kA_b D_b}\sum_{x=0}^{k-1}\left\{\left(M_b^{\text{in}}[x]\right)\sum_{y=0}^{k-x-1}\left(\left(M_b^{\text{in}}[y]\right)r_b[k-x-y-1]\right)\right\}, \quad \forall i \in \mathcal{I}_b^{\text{in}}, \forall j \in \mathcal{I}_b^{\text{out}}, \forall b \in \mathcal{P}^{\text{NGN}}, \end{aligned} \tag{24}$$

$$\sum A_{i,b}^{\text{in}} M_{b,t}^{\text{in}}[k] + \sum A_{i,b}^{\text{out}} M_{b,t}^{\text{out}}[k] = \delta_{(k,1)}(M_i^{\text{S}} - M_i^{\text{D}} - M_i^0), \quad \forall i \in \mathcal{I}^{\text{NGN}}, \forall b \in \mathcal{P}^{\text{NGN}}, \tag{25}$$

$$p_j[k] = R_b^{\mathrm{C}} p_i[k], \quad \forall i \in \mathcal{I}_b^{\text{NGN-C,in}}, j \in \mathcal{I}_b^{\text{NGN-C,out}}, \tag{26}$$

$$\frac{2c^2}{kA_{b_1}l_{b_1}}\left(M_{b_1}^{\mathrm{in}}[k-1] - M_{b_1}^{\mathrm{out}}[k-1]\right) - p_{b_1}^{\mathrm{in}}[k] = \frac{2c^2}{kA_{b_2}l_{b_2}}\left(M_{b_2}^{\mathrm{in}}[k-1] - M_{b_2}^{\mathrm{out}}[k-1]\right) - p_{b_2}^{\mathrm{in}}[k],$$
$$b_1, b_2 \in \mathcal{P}_i^{\text{NGN-infuse}}, i \in \mathcal{I}^{\text{NGN-infuse}}, \tag{27}$$

$$r_b[k] = -\frac{\sum_{x=0}^{k-1}\left(r_b[x]\left(p_b^{\mathrm{in}}[k-x] + p_b^{\mathrm{out}}[k-x]\right)\right)}{p_b^{\mathrm{in}}[0] + p_b^{\mathrm{out}}[0]}, \quad \forall b \in \mathcal{P}^{\text{NGN}}, \tag{28}$$

where $\delta_{(k,k')}$ ($\delta_{(k,0)}$ and $\delta_{(k,1)}$) is a binary parameter, $\delta_{(k,k')} = 1$ only when $k = k'$; M^0 is the initial gas injection at Node i, and $M_i^0 = \sum A_{i,b}^{\mathrm{in}} M_{b,t}[0] + \sum A_{i,b}^{\mathrm{out}} M_{b,t}[0]$; $\mathcal{I}_b^{\text{NGN-C,in}}$ and $\mathcal{I}_b^{\text{NGN-C,out}}$ are the index collections of inlet and outlet nodes of Compressor b, respectively; $\mathcal{P}_i^{\text{NGN-infuse}}$ is the index collection of pipes that flow into Node i; and $\mathcal{I}^{\text{NGN-infuse}}$ is the index collection of infuse nodes.

When the coefficients for the t, t^2, $\cdots$ and t^{k-1} terms are already known, equations (23) through (28) are a set of linear equations of unknown coefficients $M_b^{\mathrm{in}}[k]$, $M_b^{\mathrm{out}}[k]$, $p_b^{\mathrm{in}}[k]$, $p_b^{\mathrm{out}}[k]$ and $r_b[k]$. By solving these linear equations, the coefficients of the t^k terms in all holomorphic functions can be obtained.

When it is reformulated as a set of holomorphic embedded equations, Equation (27) makes the left-hand side matrix of the linear equations singular. To address this problem, for the inflowing pipes of an infuse node, we set the flow rate on the inlet equal to the outlet flow rate in the same pipe ($\frac{\mathrm{d}p_b^{\mathrm{out}}}{\mathrm{d}t} = \frac{\mathrm{d}p_b^{\mathrm{in}}}{\mathrm{d}t}$). Therefore, Equation (7) can be written as $\frac{2c^2}{A_{b_1}l_{b_1}}\left(M_{b_1}^{\mathrm{in}} - M_{b_1}^{\mathrm{out}}\right) = \frac{2c^2}{A_{b_2}l_{b_2}}\left(M_{b_2}^{\mathrm{in}} - M_{b_2}^{\mathrm{out}}\right)$. Equation (27) becomes:

$$\frac{2c^2}{A_{b_1}l_{b_1}}\left(M_{b_1}[k]^{\mathrm{in}} - M_{b_1}[k]^{\mathrm{out}}\right) = \frac{2c^2}{A_{b_2}l_{b_2}}\left(M_{b_2}[k]^{\mathrm{in}} - M_{b_2}[k]^{\mathrm{out}}\right), \quad i \in \mathcal{I}^{\text{NGN-infuse}}. \tag{29}$$

The recursive solution procedure starts from the calculation of $M_b^{\mathrm{in}}[1]$, $M_b^{\mathrm{out}}[1]$, $p_b^{\mathrm{in}}[1]$, $p_b^{\mathrm{out}}[1]$ and $r_b[1]$. Based on the germ solution ($M_b^{\mathrm{in}}[0]$, $M_b^{\mathrm{out}}[0]$, $p_b^{\mathrm{in}}[0]$, $p_b^{\mathrm{out}}[0]$ and $r_b[0]$), the coefficients for the t terms can be calculated by solving Equations (23) to (26), 28) and (29). Similarly, the coefficients of t^2, t^3, t^4, $\cdots$ in the holomorphic polynomials can be calculated by solving linear equations based on the lower-order coefficients. The unknown coefficients in the holomorphic polynomials are therefore solved order by order in the recursive paradigm below.

$$p_b^{\mathrm{in}}[0] \to p_b^{\mathrm{in}}[1] \to p_b^{\mathrm{in}}[2] \to p_b^{\mathrm{in}}[3] \cdots \to p_b^{\mathrm{in}}[n], \tag{30}$$

$$p_b^{\mathrm{out}}[0] \to p_b^{\mathrm{out}}[1] \to p_b^{\mathrm{out}}[2] \to p_b^{\mathrm{out}}[3] \cdots \to p_b^{\mathrm{out}}[n], \tag{31}$$

$$M_b^{\mathrm{in}}[0] \to M_b^{\mathrm{in}}[1] \to M_b^{\mathrm{in}}[2] \to M_b^{\mathrm{in}}[3] \cdots \to M_b^{\mathrm{in}}[n], \tag{32}$$

$$M_b^{\text{out}}[0] \rightarrow M_b^{\text{out}}[1] \rightarrow M_b^{\text{out}}[2] \rightarrow M_b^{\text{out}}[3] \cdots \rightarrow M_b^{\text{out}}[n], \tag{33}$$

$$r_b[0] \rightarrow r_b[1] \rightarrow r_b[2] \rightarrow r_b[3] \cdots \rightarrow r_b[n]. \tag{34}$$

Given the value of t, the numerical solutions of all state variables can be obtained by the solved holomorphic functions $M^{\text{in}}(t)$, $M^{\text{out}}(t)$, $p^{\text{in}}(t)$ and $p^{\text{out}}(t)$.

3.1.3. HEM Computation Scheme for NGNs

A holomorphic function of time t has a limited radius of convergence, implying that when t exceeds a certain value, the holomorphic function will diverge and no longer be valid. To address this problem, a multi-stage computation scheme [36] is adopted to guarantee the validity of the HEM-based method in performing ODE-based gas flow analysis. In this computation scheme, the state variables and the imbalance of energy flow equations are evaluated at regular time intervals. The main steps of this computation scheme are listed in Algorithm 1.

Algorithm 1 HEM computation scheme for NGNs

Input: germ solutions of $p^{\text{in}}(t)$, $p^{\text{out}}(t)$, $M^{\text{in}}(t)$, $M^{\text{out}}(t)$; pre-set criteria ϵ for the imbalance check; time span for dynamic simulation $[0, t^{\text{end}}]$ and a pre-set time interval Δt^{HEM}.

Set $t^* = 0$.
while $t^* \leq t^{\text{end}}$ **do**
    Reformulate Equations (3) to (7) using $p^{\text{in}}(t^*)$, $p^{\text{out}}(t^*)$, $M^{\text{in}}(t^*)$, $M^{\text{out}}(t^*)$.
    Calculate the unknown coefficients of the holomorphic functions recursively using Equations (23) to (26), (28) and (29).
    while $E(t^*) \leq \epsilon$ **do**
        Set $t^* = t^* + \Delta t^{\text{HEM}}$.
        Evaluate state variables $p^{\text{in}}(t^*)$, $p^{\text{out}}(t^*)$, $M^{\text{in}}(t^*)$, $M^{\text{out}}(t^*)$.
        Put the state variables into Equations (23) to (26), (28) and (29), and evaluate the imbalance $E(t^*)$ between the left side and right side.
    end while
end while

Output: the values of the state variables at the pre-set time interval; the coefficients of the holomorphic functions during the whole time span.

3.2. HE Formulation and Solution of the EPS

Although the EPS is described by a steady-state model, the operating state of EPS varies with time during a long-duration simulation. In this paper, the nodal voltage is represented by a holomorphic function ($V(t) = \sum_{n=0}^{\infty} V[n]t^n$) to show its relationship to time. The power flow equations embedding the holomorphic functions of voltage are written as follows:

$$V_i^*(t^*) \sum_k Y_{ik} V_k(t) = S_i^* - P_i^{\text{C}}(t) - S_i^{\text{change}}(t), \quad i \in \mathcal{I}^{\text{PQ}}, \tag{35}$$

$$V_i(t)V_i^*(t^*) = |V_{i,sp}|^2, \quad i \in \mathcal{I}^{\mathrm{GEN}}, \tag{36}$$

$$V_i^*(t^*)\sum_k Y_{ik}V_k(t) + V_i(t)\sum_k Y_{ik}^*V_k^*(t^*) = 2\left(P_i - P_i^{\mathrm{C}} - P_i^{\mathrm{change}}(t)\right), \quad i \in \mathcal{I}^{\mathrm{PV}}, \tag{37}$$

where $P_i^{\mathrm{C}}(t)$ is the power supplied to the power-consuming compressors at Bus i; $S_i^{\mathrm{change}}(t)$ represents the change of energy injection in Bus i; and $\mathcal{I}^{\mathrm{PQ}}$, $\mathcal{I}^{\mathrm{GEN}}$ and $\mathcal{I}^{\mathrm{PV}}$ are the index collections of PQ buses, generation buses and PV buses in the EPS, respectively.

By comparing the coefficients of the t^n terms with the same order, a set of linear equations containing the nth-order coefficients and lower-order coefficients is obtained (the detailed procedures are given in [31]). The coefficients of the holomorphic functions for nodal voltage can be calculated recursively, similar to the method in Section 3.1.2. The values of the voltage magnitude and voltage angle can be obtained by putting the time variable t into these holomorphic functions.

3.3. Computation Scheme for HEMs in IGESs

The detailed procedures of the computation scheme for IGESs are given in Algorithm 2. Similar to Algorithm 1, the HEM-based method applied in IGESs includes the reformulation of energy flow equations, a recursive solution procedure for holomorphic functions and a multi-stage computation scheme based on regular checks of energy flow equation imbalances. First, the IGES state variables are replaced by time-embedded holomorphic functions and are calculated by solving these holomorphic functions. Then, the holomorphic functions in the NGN and EPS are calculated alternately until convergence, adopting the solution procedures introduced in Sections 3.1 and 3.2. The state variables and the imbalance of the IGES equations are evaluated in the multi-stage computation scheme to perform continuous-time profiling of the IGES. The IGES computation scheme is shown in Fig. 4.

During the calculation, the holomorphic functions are expressed in the form of truncated Tayler series expansion. When the system is faced with abrupt changes or the system configuration is complicated, the convergence radius of the holomorhpic function tends to be smaller, which could cause larger errors in computation results. To guarantee the computation quality, Tayler series expansions with higher-order terms are sometimes used to reach a better approximation result. The time interval for imbalance check could be shortened to keep the computation deviation in a low level. However, this might result in greater computation burden and longer computation time. The accuracy and speed needs to be balanced in practical use.

3.4. Discussion

The most important feature of the proposed HEM method is that all the state variables are represented by time-embedded holomorphic functions, implying that the values of these variables at any time t can be obtained easily by putting t into the holomorphic functions.

Algorithm 2 HEM computation scheme for an IGES

Input: germ solutions of $p^{\text{in}}(t)$, $p^{\text{out}}(t)$, $M^{\text{in}}(t)$, $M^{\text{out}}(t)$ and $V(t)$; pre-set criteria ϵ for the imbalance check; time span for the dynamic simulation $[0, t^{\text{end}}]$ and a pre-set time interval Δt^{HEM}.

Set $t^* = 0$.
while $t^* \leq t^{\text{end}}$ **do**
    Reformulate the IGES equations (Equations (3) to (7), (8) and (9)) using $p^{\text{in}}(t^*)$, $p^{\text{out}}(t^*)$, $M^{\text{in}}(t^*)$, $M^{\text{out}}(t^*)$ and $V(t^*)$
    Calculate the unknown coefficients of the holomorphic functions in the NGN and EPS alternately until the result of the EFA at time t^* is convergent.
    while $E(t^*) < \epsilon$ **do**
        Set $t^* = t^* + \Delta t^{\text{HEM}}$.
        Calculate $p^{\text{in}}(t^*)$, $p^{\text{out}}(t^*)$, $M^{\text{in}}(t^*)$, $M^{\text{out}}(t^*)$ and $V(t^*)$.
        Evaluate $E(t^*)$ in Equations (23) to (26), (28), (29), (35) and (37).
    end while
end while

Output: the values of the state variables at the pre-set time interval; the coefficients of the holomorphic functions during the whole time span.

As shown in Fig. 5, the method that is normally adopted (e.g., the ODE-NR method mentioned in this paper) for EFA in IGESs is to solve the NGN's equations using the MATLAB ODE solver Runge-Kutta method with fixed time steps and the EPS equations using the Newton-Raphson method. This method can only provide energy flow data at a pre-set time interval, such as t_0, $t_0 + \Delta t^{\text{ODE}}$, $t_0 + 2\Delta t^{\text{ODE}}$, $\cdots$, $t_0 + (n+1)\Delta t^{\text{ODE}}$, which is still a discrete-time profiling of the whole system even when using higher resolution in the computation. The value of the operating state at other times (e.g., $t_0 + 0.5\Delta t^{\text{ODE}}$) is normally obtained via interpolation techniques or simply by running the calculation procedures again, which often brings an additional computational burden.

In contrast, the HEM adopting the multi-stage computation scheme provides a continuous-time profile by utilizing time-embedded holomorphic functions. The operating states of the IGES at any time (whether at the pre-set time interval or not) can be calculated directly by the holomorphic functions that are readily obtained, which cover all moments in the whole time span. This method checks the imbalance regularly (at times $t_0 + \Delta t^{\text{HEM}}$, $t_0 + 2\Delta t^{\text{HEM}}$, $\cdots$) to determine whether to stay in the current stage or start a new one, and the same set of holomorphic functions is used throughout the whole stage (e.g., t_0 to $\Delta t_1^{\text{HEM-STEP}}$). Holomorphic functions must be calculated only at the beginning or when the imbalance in the energy flow equations is higher than the standard, which saves considerable computational effort.

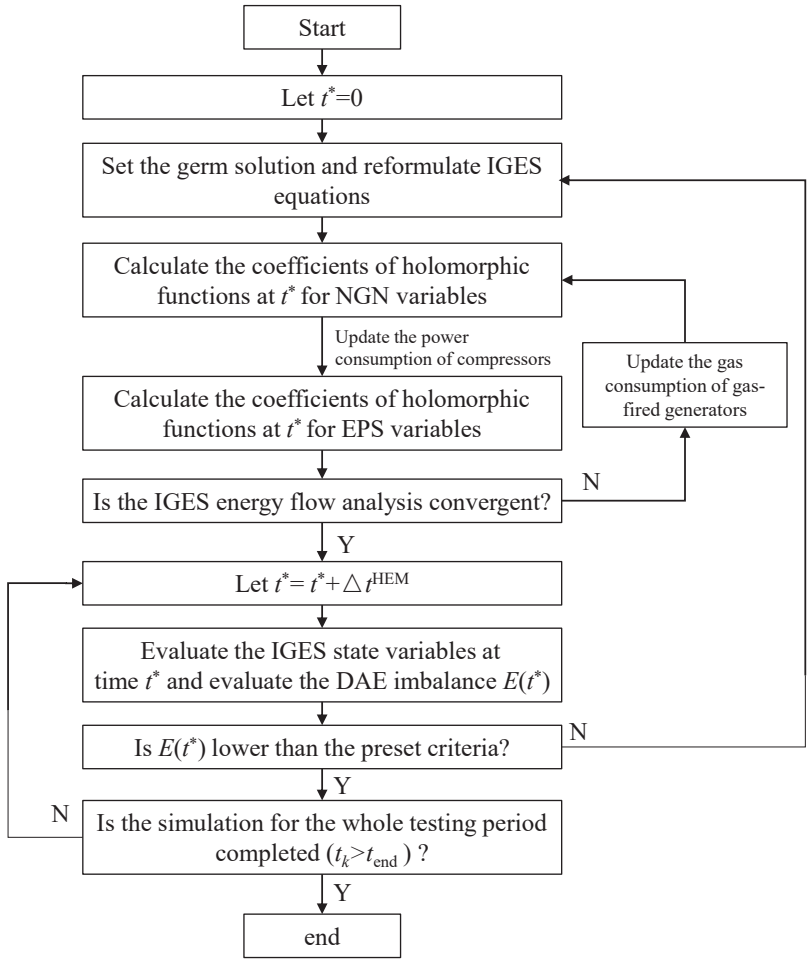

Figure 4: The HEM computation scheme considering different time scales

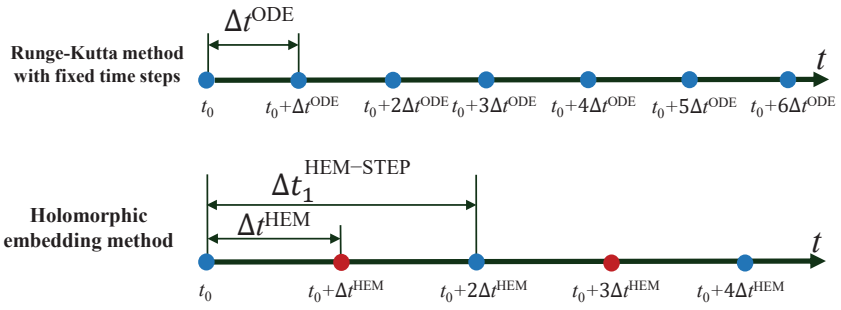

Figure 5: The comparison of computation time interval between the Runge-Kutta method and the holomorphic embedding method

4. Case Studies

Test runs are carried out in one NGN case and two IGES cases under different operating scenarios. All tests are performed on a computer with eight processors running at 3.1 GHz and 4 GB of RAM with MATLAB R2018b.

4.1. Single-pipe NGN Test Case

Before taking test runs in IGES cases, the proposed HEM method is first verified in a single-pipe NGN test case (Case I) by comparing its capability of depicting pipeline dynamics with other commonly-used methods. This case contains a source node and a load node, connected by a 2 km pipeline (as shown in Fig. 6), and different operating conditions are set during the whole simulation period to test the proposed method. The system begins with a stable operation state (no changes in supply or demand) for 100 s, then a sharp drop in demand (lasting 50 s) followed by a stable operation state for 200 s, after which the system experiences a steady increase in demand (lasting 200 s) before finally returning to the stable operation state.

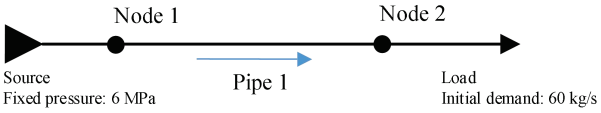

Figure 6: The configuration of the single-pipe NGN test case

Following the HEM computation scheme in Section 3.1.3, the values of IGES variables at a certain moment can be calculated by solving the unknown coefficients of holomorphic functions and then plugging time into the holomorphic functions. Taking the calculation of inlet flow rate and output pressure at 120 s as an example, the solved holomorphic functions for inlet flow rate and outlet pressure are:

$$M^{\text{in}}(t) = 58.9584 - 0.3954t - 0.0134t^2 + 7.3660 \times 10^{-4}t^3 + 1.3601 \times 10^{-5}t^4 + \cdots, \quad (38)$$

$$p^{\text{out}}(t) = 5.9910 \times 10^6 + 307.0329t - 11.7275t^2 - 0.5342t^3 + 0.0221t^4 + \cdots. \quad (39)$$

During the multi-stage computation, the HEM starts a new stage at 120 s. At 120 s, the values of M^{in} and p^{out} are equal to $M^{\text{in}}(0)$ and $p^{\text{out}}(0)$, respectively. At 121 s, the values of M^{in} and p^{out} are calculated using the same set of holomorphic functions by plugging $t = 1$ into the holomorphic functions. By repeating the steps in Algorithm 1, the values of the state variable during the whole simulation period are obtained and the system's evolution in response to disturbance can therefore be displayed.

The result of the HEM is compared with the results from the finite difference method and the ODE-NR method. The curves of the gas flow rate at the source node obtained by the finite difference method (denoted as "PDE"), the ODE-NR method (denoted as "ODE") and the HEM method (denoted as "HEM") are shown in Fig. 7 (the different operating

condistions are separated by the blue dash lines in the plot). The curve of HEM almost overlaps the curves of the two other methods, with only slight difference compared with the finite difference method. This shows that the proposed HEM method could achieve the similar computation results as other commonly-used methods do. Noted that in IGES cases or NGN cases, it usually takes a relatively long time for the finite difference method to perform a long-duration dynamic simulation with small time steps. The ODE-based method, which has been used in solving transient gas flow equations in recent years, could achieve similar performance in the dynamic simulation as the finite difference method [29]. As an alternative, the benchmark in the IGES test cases are obtained using the ODE-NR method.

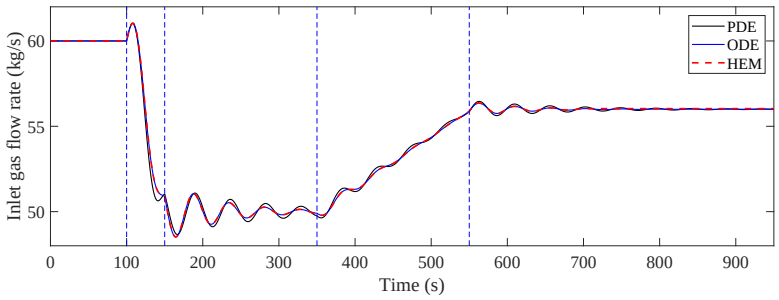

Figure 7: Simulation result comparison in Case I

4.2. Small IGES Test Case

To show the HEM's performance in IGES simulation, a test run is first carried out in a small-scale IGES case (Case II) using the proposed method. The results of the dynamic simulation are given and compared with the benchmark to show the HEM's capability of continuous-time profiling.

This case consists of an IEEE 14-bus system and a seven-node NGN. For the seven-node NGN case, there are seven nodes, six lines, two gas source nodes and one compressor. The coupling from the gas side to the power side is the power-consuming compressor on Pipe 2, which is regarded as a power load at Bus 5; the coupling from the power side to the gas side is a gas-fired generator unit at Bus 2, supported by the NGN from Node 3. The configuration of this IGES case is given in Fig. 8.

The tolerance for ODE imbalance is set to 10 for Equation (3) and 1×10^{-4} for Equation (4), and the tolerance for EPS equation mismatch is set to 1×10^{-5}. The dynamic simulation is performed under three operation scenarios:

I) an increase in the gas load at Node 1 (50% increase from 100 s to 150 s);

II) an increase in the gas load at Node 1 (20% increase from 100 s to 200 s) with an instant change in the power load at Bus 9 (30% increase at 100 s);

III) a steady increase in the power output of the gas-fired generator at Bus 2 (10 MW increase from 100 s to 200 s), which causes a simultaneous growth in the gas consumption connected to Node 3 in the NGN.

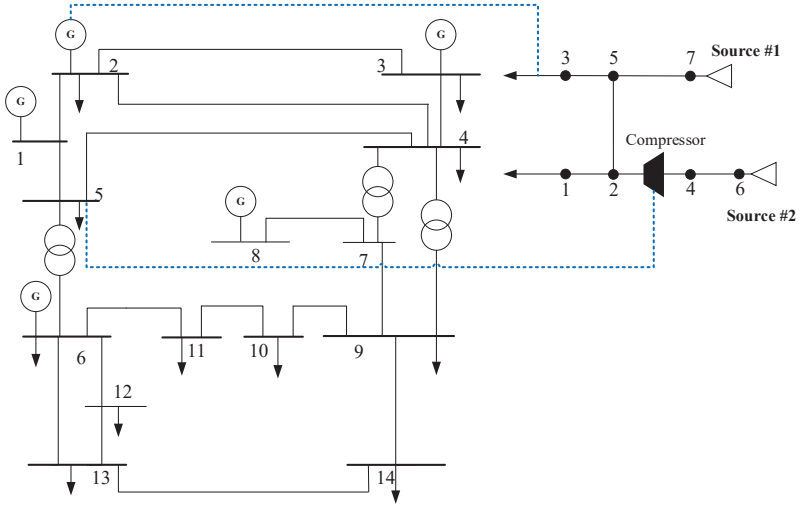

Figure 8: The configuration of the 14+7 IGES test case

4.2.1. Accuracy Analysis

To show that the HEM can provide accurate EFA outputs, the results of the HEM dynamic simulation under the three operating scenarios are shown in Figs. 9 to 11, with the benchmark data for comparison. The benchmark data are calculated using the ODE-NR method mentioned in Section 3.3, denoted as "ODE" in the legend, while the HEM result is denoted as "HEM". Each scenario can be divided into three testing stages: a steady-state stage at the beginning (the "pre-change stage", lasting 100 s), then a stage for the change in operating states in the NGN or EPS (the "interim-change stage", lasting 50 s or 100 s), and the third stage, called the "post-change stage".

In Scenario I, the fast increase in the gas load results in an obvious fluctuation in the nodal pressures and gas flow rates of all pipelines in the IGES, and it takes hundreds of seconds for the IGES to re-enter a steady state in the post-change stage. The power consumption of the compressor increases due to the sharp rise in the gas flow rate in Pipe 2, resulting in the load variation at Bus 5 in the EPS that leads to minor changes in the voltage profile of the EPS.

In Scenario II, the gas load variation is less abrupt than that in Scenario I, making all pipelines reach a new steady state in a steadier and faster way, while the EPS instantly adjusts to the power load change at Bus 9.

In Scenario III, the increasing power output of the gas-fired generators brings slightly increasing gas consumption in Node 3 and steady changes in the voltage angles, which are all reflected in the HEM results.

When the operating condition changes, the whole IGES is influenced. Even with only one gas load change in the IGES, the pressures and gas flow rates in all pipelines vary, and the variation in operating conditions in one energy sector can be transferred to the other via coupling units. During the post-change period, it takes tens to hundreds of seconds for the

Table 1: Computation Time Comparison in Case II

	ODE-NR	HEM	
Δt	$\Delta t^{\mathrm{ODE}} = 0.5$ s	$\Delta t^{\mathrm{HEM}} = 2$ s	$\Delta t^{\mathrm{HEM}} = 1$ s
Scenario I	3.276	1.294	1.568
Scenario II	3.129	1.616	1.918
Scenario III	2.723	1.197	1.360

IGES to reach a new steady state, the transient process during which needs to be depicted using the transient model rather than the steady-state model.

In all plots, the red lines and the black lines representing the HEM results and the ODE-NR results overlap almost all the time. Even when there are abrupt changes in the state variables, which means smaller radius of convergence in the holomorphic functions, the gaps between HEM result and ODE-NR result always remain low. The maximum computation deviations of nodal pressures, inlet/outlet flow rates, voltage magnitude and voltage angles stay within the range of 0.01%, 2.34%, 6×10^{-4}% and 4×10^{-3}%, respectively. This shows that the proposed method can almost provide the same output in the dynamic simulation of the IGES.

4.2.2. Computational Efficiency Analysis

To show the computational efficiency of the proposed method, the computation time of ODE-NR method and the HEM is compared. The ODE-NR method outputs discrete-time profiling of the system status every 0.5 s. The HEM method carries out a continuous-time simulation, while the imbalance of energy flow equations is checked at a certain time step (2s and 1s). To compare these two methods clearly, the HEM is required to output a discrete-time profiling which contains the values of state variables every 0.5 s during the simulation (the same output as ODE-NR when $\Delta t^{\mathrm{ODE}} = 0.5$ s). The computation time of each method is given in Tab. 1.

It takes the HEM method 1.197 s to 1.616 s to finish computation when $\Delta t^{\mathrm{HEM}} = 2$ s. When $\Delta t^{\mathrm{HEM}} = 1$ s, the computation time slightly increases. For the ODE-NR method, the computation time almost doubles compared to HEM ($\Delta t^{\mathrm{HEM}} = 1$ s). In this case, the HEM method owns a seemingly advantage in computation speed. In addition, IGES's operating states at other moments can be obtained easily using HEM's results, which further confirms HEM's high computation efficiency.

4.3. Large IGES Test Case

To validate the applicability of the proposed method in larger-scale systems, test runs are carried out in a larger case (Case III). This case consists of an IEEE 118-bus system with a 20-node NGN. The 20-node NGN case contains 20 nodes, 19 lines, six gas source nodes and one compressor [42]. The coupling relationship is built by a power-consuming compressor at Node 7 which is supported by the EPS at Bus 45, two gas-fired generator units at Buses

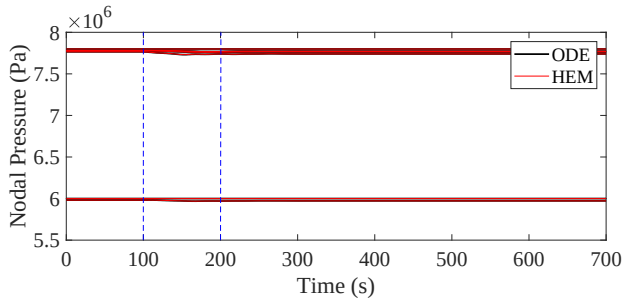

(a) Pressure comparison

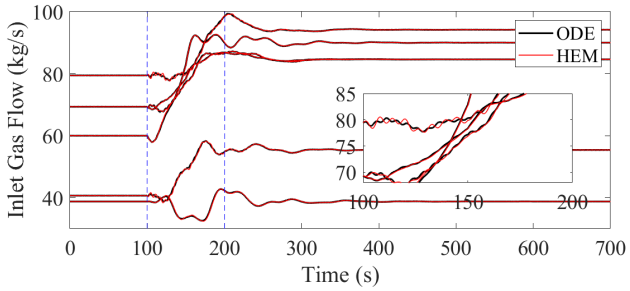

(b) Inlet flow rate comparison

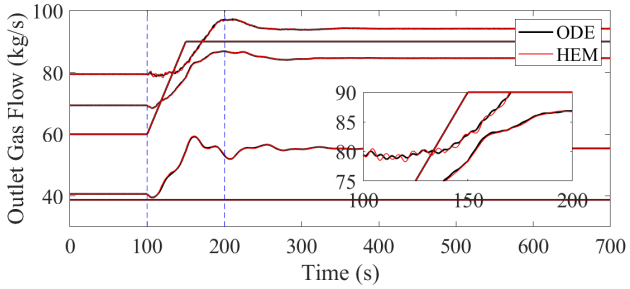

(c) Outlet flow rate comparison

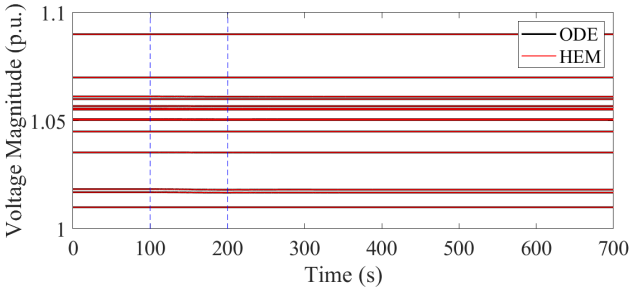

(d) Voltage magnitude comparison

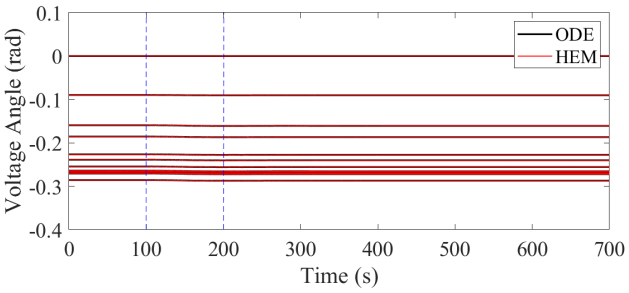

(e) Voltage angle comparison

Figure 9: Solution comparison in Scenario I, Case II

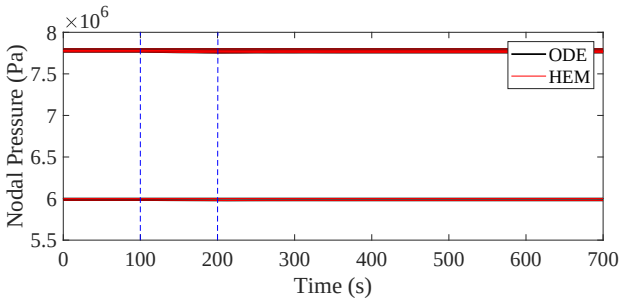

(a) Pressure comparison

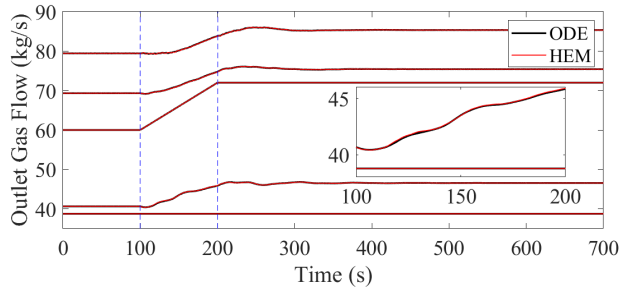

(b) Inlet flow rate comparison

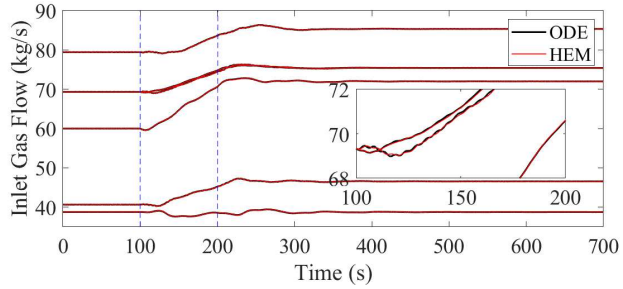

(c) Outlet flow rate comparison

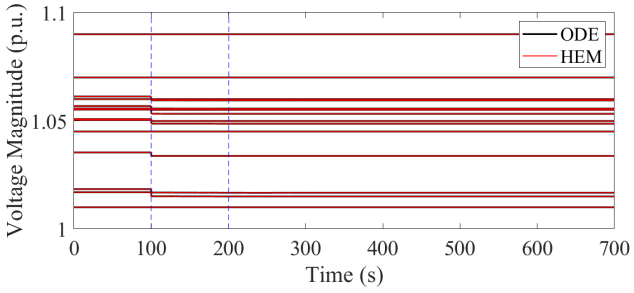

(d) tiny Voltage magnitude comparison

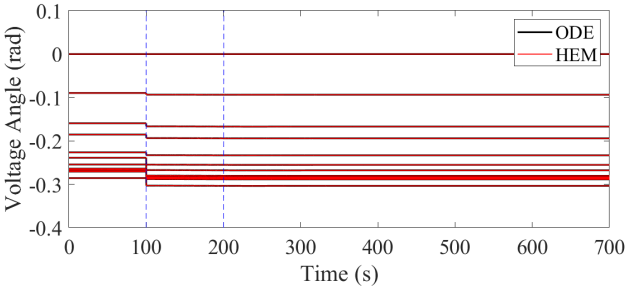

(e) Voltage angle comparison

Figure 10: Solution comparison in Scenario II, Case II

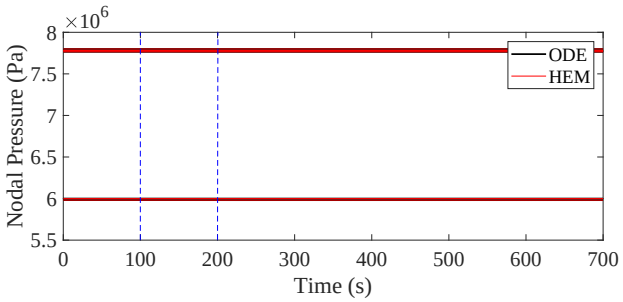

(a) Pressure comparison

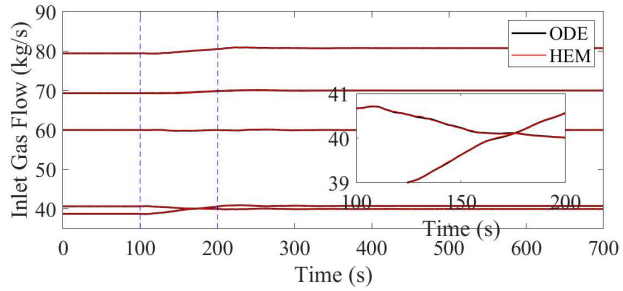

(b) Inlet flow rate comparisond

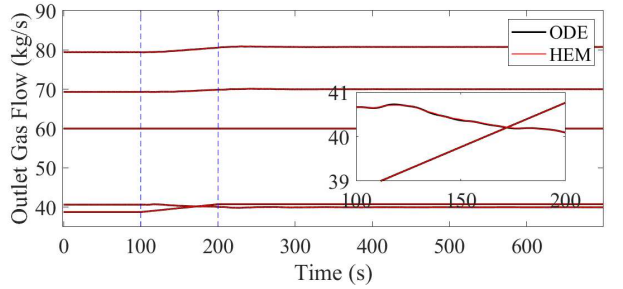

(c) Outlet flow rate comparison

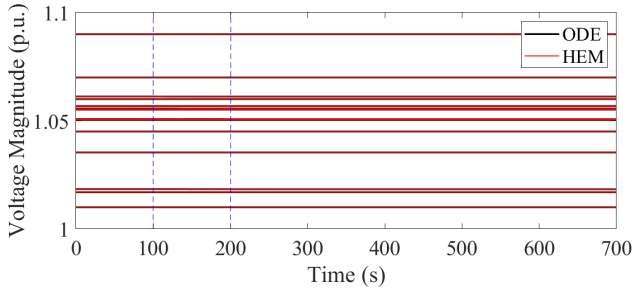

(d) Voltage magnitude comparison

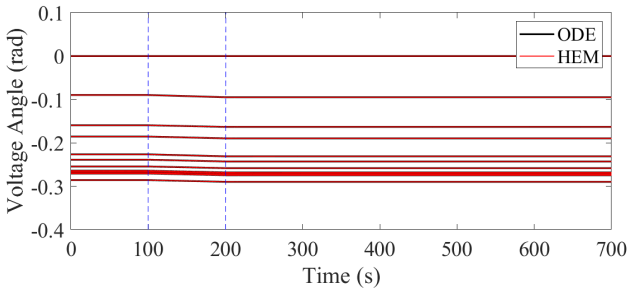

(e) Voltage angle comparison

Figure 11: Solution comparison in Scenario III, Case II

54 and 103 which are supported by the NGN at Nodes 16 and 15, and a power-to-methane equipment which is supported by the EPS at Bus 62.

During the computation, the tolerance for ODE function imbalance is set to 10 for Equation (3) and 1×10^{-4} for Equation (4), and the tolerance for EPS equation mismatch is set to 1×10^{-5}. The proposed method is tested under three operation scenarios:

I) an increase in the gas load at Node 16 (a total increase of 30 kg/s from 100 s to 200 s);

II) changes in multiple gas loads (increases of 5 kg/s and 10 kg/s at Nodes 20 and 16 from 100 s to 200 s; a decrease of -20 kg/s at Node 15 from 100 s to 200 s);

III) changes in multiple gas loads (a decrease of 5 kg/s at Node 7 and an increase of 6 kg/s at Node 10 from 100 s to 200 s) and changes in the power output of gas-fired generators (a decrease of 10 MW for the generator at Bus 54 and an increase of 15 MW for the generator at Bus 103 from 100 s to 200 s).

4.3.1. Accuracy Analysis

To analyze the accuracy of the HEM, the simulation results are compared with the ODE-NR benchmark results, and the maximum and mean deviations of the proposed method during the whole time span are shown in Fig. 12. During the interim-change stage (100 s to 200 s), the deviations are obviously larger due to the change in operating conditions. This is because the abrupt changes in operating conditions hinder the holomorphic functions in the proposed method in obtaining an accurate approximation of the IGES state variables. After the load/supply variation stops, the deviations gradually decrease as the IGES approaches the new steady state.

For all scenarios, the maximum deviations of the nodal pressures, gas flow rates and voltage magnitudes are 0.0032%, 3.3202% and 0.0024%, which show that the HEM results are similar to the ODE-NR results. This validates that the HEM could reliably generate simulation results in larger case.

4.3.2. Computational Efficiency Analysis

The computation time of the HEM method and the ODE-NR method is given in Tab. 2. The ODE-NR method generates discrete-time profilings at different time intervals (2 s, 1 s, and 0.5 s) and the HEM method output continuous-time profiling with regular imbalance check at different time intervels (2 s and 1 s). For both methods, the computation time grows when a smaller time interval is used. It takes the HEM method 7.871 s to 8.190 s to finish computation when $\Delta t^{\mathrm{HEM}} = 2$ s, and the figures almost double when $\Delta t^{\mathrm{HEM}} = 1$ s. For the ODE-NR method, the computation time is approximately 6.6 s for Scenarios I and II and 8.5 s for Scenario III. The computation speeds for both methods are slowed down by smaller Δt. When the time resolution of the simulation result is no higher than 1 s, the HEM costs around 8 s (using $\Delta t^{\mathrm{HEM}} = 2$ s) while the ODE-NR method costs more than 10 s. This is mainly because the HEM is less affected in computation speed since the additional computation time is only spent on plugging more time into holomorphic functions, rather than repeatedly solving DAEs and nonlinear algebraic equations. Though the speed advantage of the HEM in larger IGES case is not as obvious as Case II, the proposed method

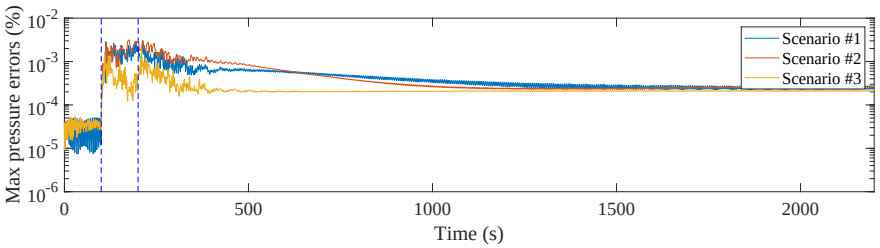

(a) Max Error in Nodal Pressure

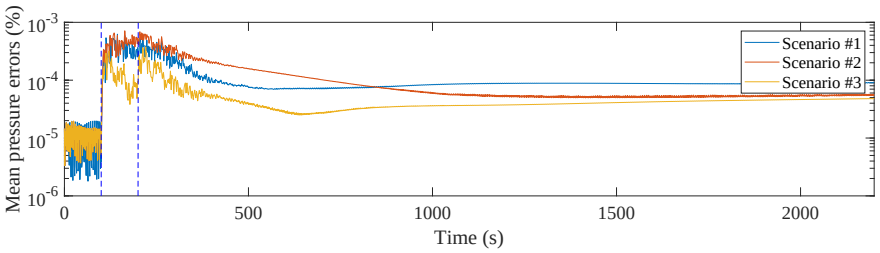

(b) Mean Error in Nodal Pressure

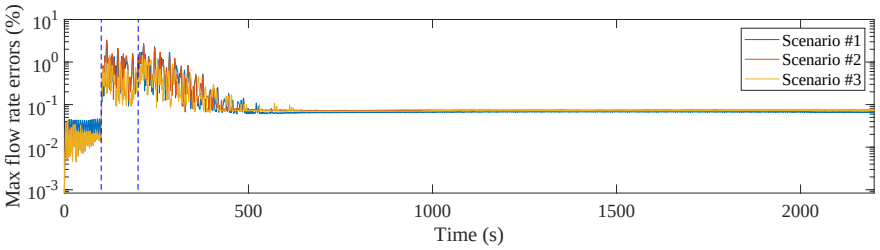

(c) Max Error in Mass Flow Rate

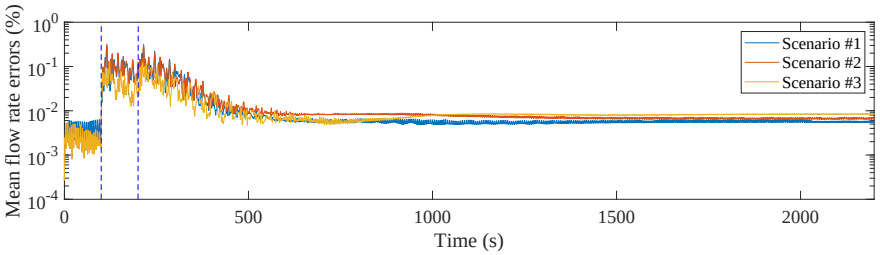

(d) Mean Error in Mass Flow Rate

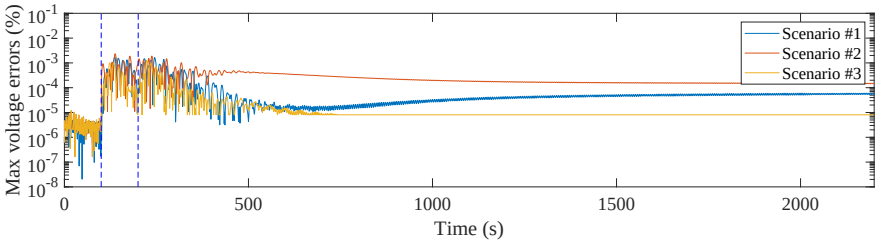

(e) Max Error in Voltage Magnitude

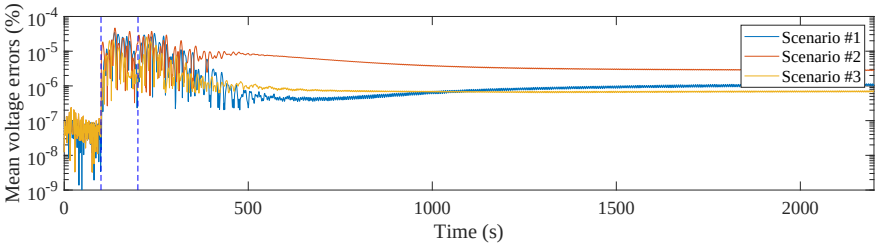

(f) Mean Error in Voltage Magnitude

Figure 12: Computation Error in Case III

Table 2: Computation Time Comparison in Case III

	ODE-NR method			HEM method	
Δt (s)	2	1	0.5	2	1
Scenario I	6.5748	13.0913	22.5898	8.1902	16.3073
Scenario II	6.6606	13.1397	22.6229	7.8705	15.4137
Scenario III	8.5744	14.4625	24.8917	7.9911	15.1081

is still more flexible and efficient in computational performance considering its capability of providing energy flow solution at any time t.

5. Conclusion

This paper proposes a dynamic energy flow analysis method for IGESs based on the holomorphic embedding method. An NGN model in the form of DAEs is adopted to depict the pipeline dynamics. The original energy flow equations in the IGES are reconstructed using holomorphic functions and the time variable t. Then, an HEM-based analysis algorithm is developed based on a novel solution method of the DAE system using holomorphic embedding and a multi-stage computation scheme. The proposed energy flow analysis method can be used in the dynamic simulation of IGESs, especially under potential disturbances from the load/supplier side, providing continuous-time profiling of the system operating states in an accurate and efficient way. The results of the case studies demonstrate that the proposed method can generate similar energy flow solutions as the normally used method. The proposed method is also more flexible and efficient in energy flow computation when the computation time interval is smaller or energy flow profiles at other times are needed. Considering the HEM's capability in reflecting time-varying state variables, its future work should include further exploitation of the proposed method, such as a reliability study of IGESs based on the holomorphic embedding method, and its wider application in other systems, such as district heating/cooling networks. Further improvement in the comptutational performance should be studied as well.

6. Acknowledgments

This work was funded by the National Natural Science Foundation of China (Grant No. 52177086), the Natural Science Foundation of Guangdong Province (No. 2019A1515011408), and the Pearl River Talent Program of Guangdong Province (No. 2017GC010467).

Appendix A. Nomenclature

See Tables 3 - 6.

Table 3: Abbreviations

Acronym	Full form
DAE	Differential algebraic equation
EFA	Energy flow analysis
EPS	Electric power system
HEM	Holomorphic embedding method
IGES	Integrated gas and electricity system
NG	Natural gas
NGN	Natural gas network
ODE	Ordinary differential equation
PDE	Partial differential equation

Table 4: Indice collections

Notation	Definition
$\mathcal{I}^{\text{EPS}}$	Index collection of buses in EPS
$\mathcal{I}^{\text{GEN}}$	Index collection of generation buses
$\mathcal{I}^{\text{NGN}}$	Index collection of nodes in NGN
$\mathcal{I}_b^{\text{NGN-C,in}}$	Index collection of inlet nodes of Compressor b in NGN
$\mathcal{I}_b^{\text{NGN-C,out}}$	Index collection of outlet nodes of Compressor b in NGN
$\mathcal{I}^{\text{NGN-infuse}}$	Index collection of infuse nodes
$\mathcal{I}^{\text{PQ}}$	Index collection of PQ buses
$\mathcal{I}^{\text{PV}}$	Index collection of PV buses
$\mathcal{P}^{\text{NGN}}$	Index collection of pipelines in NGN
$\mathcal{P}^{\text{NGN-COMP}}$	Index collection of pipes installed with compressor in NGN
$\mathcal{P}_i^{\text{NGN-infuse}}$	Index collection of pipes that flow into Node i
$\mathcal{T}$	Index collection of time periods

Table 5: Parameters

Parameter	Definition
A_b	pipe cross-sectional area of Pipe b (m^2)
A^{in}	The nodal-line incidence matrix for inflowing pipelines in NGN
A^{out}	The nodal-line incidence matrix for outlowing pipelines in NGN
B	The susceptance matrix in EPS (S)
c	sound velocity in gas (m/s)
$C_{b,t}^{\text{C}}$	Coefficient of compressor's power consumption of Pipe b at time t (kg/MWs)
$C_{i,t}^{\text{P2M}}$	Coefficient of power to methane ratio of Bus i at time t (kg/MWs)
D_b	Pipe diameter of Pipe b at time t (m)
G	The conductance matrix in EPS (S)
l_b	Length of Segment/Pipe b (m)
$R_{b,t}^{\text{C}}$	Compression ratio of the compresor on Pipe b at time t (kg/Pa)
α_i	Coefficient of the gas consumtion of the ith gas turbine ($\text{kg/MW}^2\text{s}$)
β_i	Coefficient of the gas consumtion of the ith gas turbine (kg/MWs)
γ_i	Coefficient of the gas consumtion of the ith gas turbine (kg/s)
$\delta_{(k,k')}$	Binary parameter determined by k and k'
λ_b	Coefficient of pipe roughness of Pipe b

Table 6: Variables

Variable	Definition
M	Gas flow rate (kg/s)
$M_{k,t}^{\mathrm{C}}$	gas flow rate through the pipe equipped with Compressor k at time t (kg/s)
$M_{i,t}^{\mathrm{D}}$	Gas demand of Node i at time t (kg/s)
$M_{k,t}^{\mathrm{GT}}$	Gas consumption of Turbine k at time t (kg/s)
M_b^{in}	The gas flow rates at the inlet of Segment/Pipe b (kg/s)
$M_b^{\mathrm{in}}[n]$	Coefficient of the t^n term in holomorphic function $p_b^{\mathrm{in}}(t)$
M_b^{out}	The gas flow rates at the outlet of Segment/Pipe b (kg/s)
$M_b^{\mathrm{out}}[n]$	Coefficient of the t^n term in holomorphic function $M_b^{\mathrm{out}}(t)$
$M_{i,t}^{\mathrm{P2M}}$	The methane output of power-to-methane equipment of But i at time t (kg/s)
$M_{i,t}^{\mathrm{S}}$	Gas supply of Node i at time t (kg/s)
M_i^0	Initial gas injection of Node i (kg/s)
p	Gas pressure (Pa)
$P_{i,t}^{\mathrm{C}}$	Power comsumption of the compressor supplied by Bus i at time t (MW)
P_i^{G}	Active power generation of Bus i (MW)
p_b^{in}	Pressure on the inlet Segment/Pipe b (Pa)
$p_b^{\mathrm{in}}[n]$	Coefficient of the t^n term in holomorphic function $p_b^{\mathrm{in}}(t)$
p_b^{out}	Pressure on the outlet Segment/Pipe b (Pa)
$p_b^{\mathrm{out}}[n]$	Coefficient of the t^n term in holomorphic function $p_b^{\mathrm{out}}(t)$ (Pa)
P_i^{L}	Active power consumption of Bus i (MW)
$P_{k,t}^{\mathrm{GT}}$	Power output of Turbine k at time t (MW)
$P_{i,t}^{\mathrm{P2M}}$	Power consumption of power-to-methane equipment of Bus i at time t (MW)
Q_i^{G}	Reactive power generation of Bus i (MW)
Q_i^{L}	Reactive power consumption of Bus i (MW)
$r_b\,[n]$	Coefficient of the t^n term in holomorphic function $r_b(t)$
t	Time (s)
V_i	Voltage of Bus i (p.u.)
θ_i	Voltage angle of Bus i (rad)

References

[1] Department for Business EIS. Uk energy statistics statistical press release - september 2020. https://assets.publishing.service.gov.uk/government/uploads/system/uploads/attachment_data/file/921895/Press_Notice_September_2020.pdf; 2020.

[2] Administration UEI. Us energy facts explained. https://www.eia.gov/energyexplained/us-energy-facts; 2020.

[3] Zhou H, Zheng J, Li Z, Wu Q, Zhou X. Multi-stage contingency-constrained co-planning for electricity-gas systems interconnected with gas-fired units and power-to-gas plants using iterative benders decomposition. Energy 2019;180:689–701.

[4] Yang H, You P, Shang C. Distributed planning of electricity and natural gas networks and energy hubs. Applied Energy 2021;282:116090.

[5] Sun Y, Zhang B, Ge L, Sidorov D, Wang J, Xu Z. Day-ahead optimization schedule for gas-electric integrated energy system based on second-order cone programming. CSEE Journal of Power and Energy Systems 2020;6(1):142–51. doi:10.17775/CSEEJPES.2019.00860.

[6] Song X, Wang Y, Zhang Z, Shen C, Peña-Mora F. Economic-environmental equilibrium-based bi-level dispatch strategy towards integrated electricity and natural gas systems. Applied Energy 2021;281:116142.

[7] Bao M, Ding Y, Singh C, Shao C. A multi-state model for reliability assessment of integrated gas and power systems utilizing universal generating function techniques. IEEE Transactions on Smart Grid 2019;10(6):6271–83.

[8] Juanwei C, Tao Y, Yue X, Xiaohua C, Bo Y, Baomin Z. Fast analytical method for reliability evaluation of electricity-gas integrated energy system considering dispatch strategies. Applied Energy 2019;242:260–72.

[9] Martinez-Mares A, Fuerte-Esquivel CR. A unified gas and power flow analysis in natural gas and electricity coupled networks. IEEE Transactions on Power Systems 2012;27(4):2156–66.

[10] Meng Q, Guan Q, Jia N, Zhang L, Wang Y. An improved sequential energy flow analysis method based on multiple balance nodes in gas-electricity interconnection systems. IEEE Access 2019;7:95487–95.

[11] Vidović D, Sutlović E, Majstrović M. Steady state analysis and modeling of the gas compressor station using the electrical analogy. Energy 2019;166:307–17.

[12] Schwele A, Ordoudis C, Kazempour J, Pinson P. Coordination of power and natural gas systems: Convexification approaches for linepack modeling. In: 2019 IEEE Milan PowerTech. IEEE; 2019, p. 1–6.

[13] Pambour KA, Erdener BC, Bolado-Lavin R, Dijkema GP. Saint–a novel quasi-dynamic model for assessing security of supply in coupled gas and electricity transmission networks. Applied energy 2017;203:829–57.

[14] Chen Y, Yao Y, Lin Y, Yang X. Dynamic state estimation for integrated electricity-gas systems based on kalman filter. CSEE Journal of Power and Energy Systems 2020;:1–11doi:10.17775/CSEEJPES.2020.02050.

[15] Zheng C, Fang J, Wang S, Ai X, Liu Z, Chen Z. Energy flow optimization of integrated gas and power systems in continuous time and space. IEEE Transactions on Smart Grid 2021;12(3):2611–24. doi:10.1109/TSG.2020.3044609.

[16] Qiu Y, Grundel S, Stoll M, Benner P. Efficient numerical methods for gas network modeling and simulation. https://www.researchgate.net/publication/326507086_Efficient_Numerical_Methods_for_Gas_Network_Modeling_and_Simulation; 2018.

[17] Olorunmaiye J, Imide N. Computation of natural gas pipeline rupture problems using the method of characteristics. Journal of hazardous materials 1993;34(1):81–98.

[18] Egger H. A robust conservative mixed finite element method for isentropic compressible flow on pipe networks. SIAM Journal on Scientific Computing 2018;40(1):A108–29.

[19] Kiuchi T. An implicit method for transient gas flows in pipe networks. International Journal of Heat and Fluid Flow 1994;15(5):378–83.

[20] Helgaker JF, Müller B, Ytrehus T. Transient flow in natural gas pipelines using implicit finite difference schemes. Journal of Offshore Mechanics and Arctic Engineering 2014;136(3).
[21] Su H, Zio E, Zhang ZJ, Xiong CZ, Dai QS, Wu QW, et al. Development of an integrated dynamic model for supply security and resilience analysis of natural gas pipeline network systems. Petroleum Science 2021;.
[22] Fakhroleslam M, Bozorgmehry Boozarjomehry R, Sahlodin AM, Sin G, Mansouri SS. Dynamic simulation of natural gas transmission pipeline systems through autoregressive neural networks. Industrial & Engineering Chemistry Research 2021;60(27):9851–9.
[23] Zhou Y, Gu C, Wu H, Song Y. An equivalent model of gas networks for dynamic analysis of gas-electricity systems. IEEE Transactions on Power Systems 2017;32(6):4255–64.
[24] Tentis E, Margaris D, Papanikas D. Transient gas flow simulation using an adaptive method of lines. Comptes Rendus Mecanique 2003;331(7):481–7.
[25] Corraro F, Verde L. A component oriented modelling approach for fluid-dynamic piping system simulation (fluidys). In: CACSD. Conference Proceedings. IEEE International Symposium on Computer-Aided Control System Design (Cat. No. 00TH8537). IEEE; 2000, p. 214–9.
[26] Tao W, Ti H. Transient analysis of gas pipeline network. Chemical Engineering Journal 1998;69(1):47–52.
[27] Zlotnik A, Dyachenko S, Backhaus S, Chertkov M. Model reduction and optimization of natural gas pipeline dynamics. In: Dynamic Systems and Control Conference; vol. 57267. American Society of Mechanical Engineers; 2015, p. V003T39A002.
[28] Chen Y, Guo Q, Sun H, Pan Z, Chen B. Generalized phasor modeling of dynamic gas flow for integrated electricity-gas dispatch. Applied Energy 2021;283:116153.
[29] Chevalier S, Wu D. Dynamic linepack depletion models for natural gas pipeline networks. arXiv preprint arXiv:200111496 2020;.
[30] Trias A. The holomorphic embedding load flow method. In: 2012 IEEE Power and Energy Society General Meeting. IEEE; 2012, p. 1–8.
[31] Chiang HD, Wang T, Sheng H. A novel fast and flexible holomorphic embedding power flow method. IEEE Transactions on Power Systems 2017;33(3):2551–62.
[32] Rao SD, Tylavsky DJ, Feng Y. Estimating the saddle-node bifurcation point of static power systems using the holomorphic embedding method. International Journal of Electrical Power & Energy Systems 2017;84:1–12.
[33] Wu D, Wang B. Holomorphic embedding based continuation method for identifying multiple power flow solutions. IEEE Access 2019;7:86843–53.
[34] Liu C, Wang B, Hu F, Sun K, Bak CL. Online voltage stability assessment for load areas based on the holomorphic embedding method. IEEE Transactions on Power Systems 2017;33(4):3720–34.
[35] Zhu Y, Tylavsky D, Rao S. Nonlinear structure-preserving network reduction using holomorphic embedding. IEEE Transactions on Power Systems 2017;33(2):1926–35.
[36] Yao R, Sun K, Shi D, Zhang X. Voltage stability analysis of power systems with induction motors based on holomorphic embedding. IEEE Transactions on Power Systems 2019;34(2):1278–88.
[37] Yao R, Liu Y, Sun K, Qiu F, Wang J. Efficient and robust dynamic simulation of power systems with holomorphic embedding. IEEE Transactions on Power Systems 2019;35(2):938–49.
[38] Asl DK, Seifi AR, Rastegar M, Mohammadi M. Optimal energy flow in integrated energy distribution systems considering unbalanced operation of power distribution systems. International Journal of Electrical Power & Energy Systems 2020;121.
[39] Zhang T, Li Z, Zheng J, Wu Q, Zhou X. Power flow analysis of integrated gas and electricity systems using the fast and flexible holomorphic embedding method. In: 2020 IEEE Power Energy Society General Meeting (PESGM). 2020, p. 1–5. doi:10.1109/PESGM41954.2020.9281987.
[40] Pan Z, Guo Q, Sun H. Interactions of district electricity and heating systems considering time-scale characteristics based on quasi-steady multi-energy flow. Applied Energy 2016;167(apr.1):230–43.
[41] Rao S, Feng Y, Tylavsky DJ, Subramanian MK. The holomorphic embedding method applied to the power-flow problem. IEEE Transactions on Power Systems 2015;31(5):3816–28.

[42] De Wolf D, Smeers Y. The gas transmission problem solved by an extension of the simplex algorithm. CORE Discussion Papers RP 2000;.